

RESEARCH ARTICLE

The Effects of Thermal Radiation on an Unsteady MHD Axisymmetric Stagnation-Point Flow over a Shrinking Sheet in Presence of Temperature Dependent Thermal Conductivity with Navier Slip

Sabyasachi Mondal*, Nageeb A. H. Haroun, Precious Sibanda

University of KwaZulu-Natal, School of Mathematics, Statistics and Computer Science, Private Bag X01, Scottsville, Pietermaritzburg 3209, South Africa

* sabya.mondal.2007@gmail.com



OPEN ACCESS

Citation: Mondal S, Haroun NAH, Sibanda P (2015) The Effects of Thermal Radiation on an Unsteady MHD Axisymmetric Stagnation-Point Flow over a Shrinking Sheet in Presence of Temperature Dependent Thermal Conductivity with Navier Slip. PLoS ONE 10(9): e0138355. doi:10.1371/journal.pone.0138355

Editor: Saeed Islam, Abdul Wali Khan University Mardan Pakistan, PAKISTAN

Received: April 24, 2015

Accepted: August 29, 2015

Published: September 28, 2015

Copyright: © 2015 Mondal et al. This is an open access article distributed under the terms of the [Creative Commons Attribution License](#), which permits unrestricted use, distribution, and reproduction in any medium, provided the original author and source are credited.

Data Availability Statement: All the data underlying the findings are fully available without restriction.

Funding: This work is funded by the University of KwaZulu-Natal through SM's postdoctoral fellowship.

Competing Interests: The authors have declared that no competing interests exist.

Abstract

In this paper, the magnetohydrodynamic (MHD) axisymmetric stagnation-point flow of an unsteady and electrically conducting incompressible viscous fluid in with temperature dependent thermal conductivity, thermal radiation and Navier slip is investigated. The flow is due to a shrinking surface that is shrunk axisymmetrically in its own plane with a linear velocity. The magnetic field is imposed normally to the sheet. The model equations that describe this fluid flow are solved by using the spectral relaxation method. Here, heat transfer processes are discussed for two different types of wall heating; (a) a prescribed surface temperature and (b) a prescribed surface heat flux. We discuss and evaluate how the various parameters affect the fluid flow, heat transfer and the temperature field with the aid of different graphical presentations and tabulated results.

1 Introduction

The study of an unsteady fluid flow toward a stretching/shrinking sheet has great importance due to its various applications in science and engineering. Some often given examples in this regard include metal rolling, drawing and pultrusion. Heat transfer in such flows with both constant and variable wall temperature was investigated by Gupta and Gupta [1] and also investigated by Carragher and Crane [2]. Work on unsteady MHD flow with ramped wall temperature has been done by Khan et al. [3], Samiulhaq [4] and Khalid [5]. Wang [6] investigated the steady flow through a flat surface of a viscous fluid which is stretched in its own plane in two perpendicular directions. MHD free convection of unsteady flow in a porous medium with Newtonian heating and constant mass diffusion was studied by Hussanan [7]. Pavlov [8] studied exact similarity solution of the steady two-dimensional boundary layer flow equations in presence of magnetic field of an electrically conducting fluid due to the stretching of an elastic

surface in the presence of a uniform transverse magnetic field. Mabood et al. [9] solved the differential equations of the model flow and heat transfer in an axisymmetric channel using the optimal homotopy asymptotic method. Homann [10] studied three dimensional axisymmetric stagnation-point flow using a similarity transform for reducing the Navier-Stokes equations to third order ordinary differential equations.

Chiam [11] investigated steady axisymmetric stagnation-point flow of a viscous fluid over an axisymmetrically stretched surface. Mahapatra and Gupta [12] examined axisymmetric stagnation-point flow of an incompressible viscous fluid towards a stretching surface. Axisymmetric stagnation-point flow in presence of a uniform magnetic field towards a stretching surface with heat generation was investigated by Attia [13].

Considerable interest has been shown on the boundary layer flow over a shrinking sheet in recent years. Some of the applications of the shrinking sheet problem in industry relate to the shrinking film that is can be unwrapped easily with adequate heat and used in the packaging of bulk products. The shrinking fluid flow study, which is essentially a backward flow, can also be applied to the study of hydraulic properties of agricultural clay soils, capillary effects in the shrinking-swell behaviour and small pores. The related changes in mechanical and hydraulic studies of such soils have a significant impact on the behaviour and the transport properties of the fluid. The fluid loses the memory of the perturbation produced by the slot for this backward flow configuration. Due to this reason, the fluid flow due to a shrinking sheet has some quite distinct physical characteristics compared to the forward stretching case.

Miklavcic and Wang [14] studied axisymmetric flow with uniform suction induced by a shrinking surface. Wang [15] examined heat transfer from a shrinking sheet due to a steady two-dimensional axisymmetric stagnation-point flow. Qasim et al. [16] examined heat transfer in the case of a micropolar fluid through a stretching sheet with Newtonian heating. Recently, Mahapatra and Nanday [17] studied heat transfer in an axisymmetric stagnation-point flow in the presence of a magnetic field. Qayyum et al. [18] presented an analysis of unsteady axisymmetric squeezing fluid flow with slip boundary conditions through a porous channel. Some recent studies of boundary layer flow in presence of a magnetic field include those of Mabood and his group [19–21]. For the case of a nonlinearly stretching sheet, we note the work of Khan et al. [22].

In this paper, we generalize the study of MHD fluid flow with an unsteady conditions through a shrinking sheet including a temperature dependent thermal conductivity, radiation and a Navier slip condition. The surface with prescribed surface temperature (PST) and surface with prescribed wall heat flux (PHF) are considered as two examples of non-isothermal boundary conditions.

Ethical Statement: This study involved only numerical simulations and the analysis of fluid flow.

2 Formulation

Here, we consider the unsteady axisymmetric stagnation-point flow of an electrically conducting incompressible fluid from the surface which is shrunk axisymmetrically. We have used Cartesian axes instead of cylindrical axes due to possible non-alignment, Wang [15]. The flow configuration is shown in Fig 1. In this frame of reference, let the velocity components are u , v and w in the x - direction, y - direction and z -direction, respectively.

At the surface the fluid velocity components are

$$u = \frac{(l+x)c}{1-\lambda t}, \quad v = \frac{cy}{1-\lambda t} \quad \text{and} \quad w = 0,$$

where $-l$ is the location of the origin and $c (< 0)$ denotes the shrinking rate (and if $c > 0$ the it

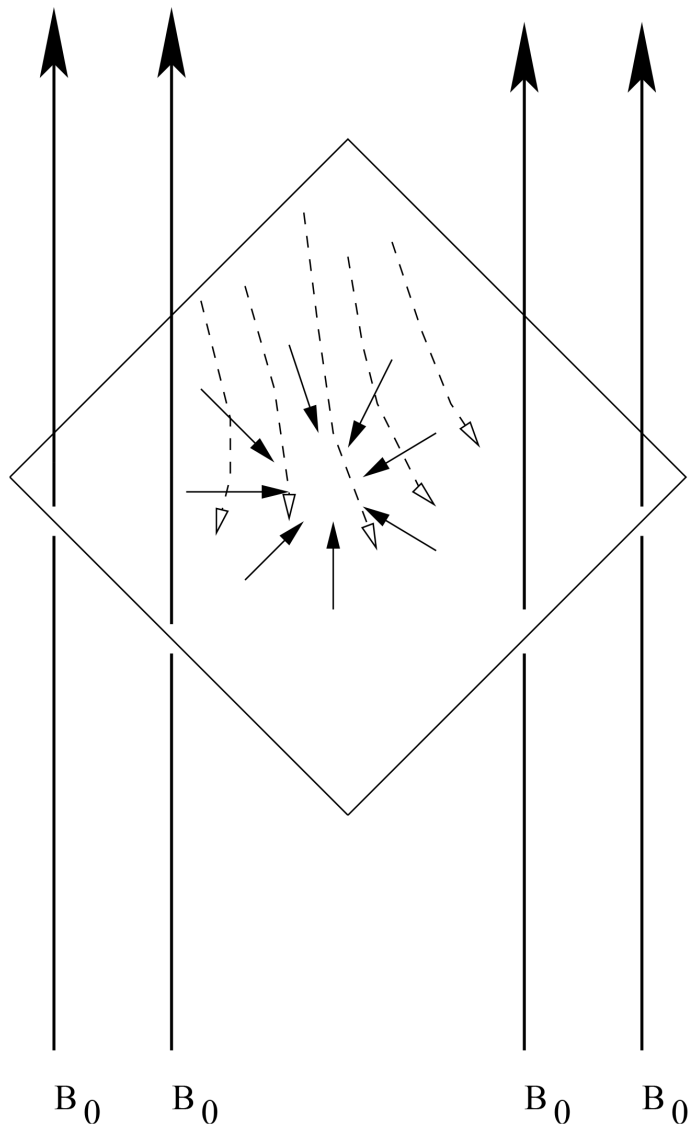


Fig 1. A sketch of the physical problem.

doi:10.1371/journal.pone.0138355.g001

denotes stretching rate). Here the sheet shrinkage is along the negative x -axis. Note that the stretching axis and the point flow are not always aligned (that is, $l \neq 0$).

The velocity components in the ambient region are given by

$$U = \frac{ax}{1 - \lambda t}, \quad V = \frac{ay}{1 - \lambda t} \quad \text{and} \quad W = -\frac{2az}{1 - \lambda t},$$

where a (> 0) is a constant that is a measure of the strength of the stagnation-point flow and λ quantifies the unsteadiness of the problem. For a decelerating shrinking sheet $\lambda < 0$ whereas for an accelerating sheet $\lambda > 0$. The magnetic field B_0 is imposed in the normal direction to the surface i.e., parallel to z -axis.

The continuity and momentum equations are (Bansal [23])

$$\frac{\partial u}{\partial x} + \frac{\partial v}{\partial y} + \frac{\partial w}{\partial z} = 0, \quad (1)$$

$$\frac{\partial u}{\partial t} + u \frac{\partial u}{\partial x} + w \frac{\partial u}{\partial z} = -\frac{1}{\rho} \frac{\partial p}{\partial x} + v \frac{\partial^2 u}{\partial z^2} - \frac{\sigma B_0^2 u}{\rho}. \quad (2)$$

The pressure gradient in the free stream can be obtained from [Eq \(2\)](#) as

$$\frac{1}{\rho} \frac{\partial p}{\partial x} = -\frac{\partial U}{\partial t} - U \frac{\partial U}{\partial x} - \frac{\sigma B_0^2 U}{\rho}, \quad (3)$$

so that [Eq \(2\)](#) becomes

$$\frac{\partial u}{\partial t} + u \frac{\partial u}{\partial x} + w \frac{\partial u}{\partial z} = \frac{\partial U}{\partial t} + U \frac{\partial U}{\partial x} + v \frac{\partial^2 u}{\partial z^2} + \frac{\sigma B_0^2}{\rho} (U - u). \quad (4)$$

The appropriate boundary conditions with velocity partial slip are given by (see Jat and Rajotia [24]);

$$u = u_w(x, t) + L_1 v \frac{\partial u}{\partial z}, \quad v = cy/(1 - \lambda t), \quad w = 0 \quad \text{at} \quad z = 0, \quad (5)$$

$$u \rightarrow U(x, t) = ax/(1 - \lambda t), \quad \text{as} \quad z \rightarrow \infty. \quad (6)$$

where $a (> 0)$ is a constant. For the u -component boundary condition, we have assumed a velocity slip. This is proportional to local shear stress with slip factor $L_1 = L(1 - \lambda t)^{1/2}$ where L is the initial velocity. Note that the essential slip factor L_1 changes with time and has dimensions (velocity) $^{-1}$. The velocity

$$u_w(x, t) (= c(x + l)/(1 - \lambda t)), \quad (7)$$

is valid for time $t < \lambda^{-1}$.

We introduce the following similarity transformations to transform the governing equations

$$u = \frac{[ax f'(\eta) + c l h(\eta)]}{1 - \lambda t}, \quad v = \frac{ay f'(\eta)}{1 - \lambda t}, \quad w = -2 \sqrt{\frac{av}{1 - \lambda t}} f(\eta), \quad (8)$$

where

$$\eta = z \left(\frac{a}{v(1 - \lambda t)} \right)^{1/2}, \quad (9)$$

and differentiation is with respect to η . Eqs (8) and (1) is identically satisfied. Substituting Eqs (8) and (9) in [Eq \(4\)](#) and equating the coefficients of x^0 and x^1 , we obtain the coupled non-linear differential equations

$$f''' + 2ff'' - f^2 + 1 + M^2(1 - f') - \beta \left[\frac{\eta}{2} f'' + f' - 1 \right] = 0, \quad (10)$$

$$h'' + 2fh' - hf' - M^2h - \beta \left[\frac{\eta}{2} h' + h \right] = 0, \quad (11)$$

where $B = B_0 \sqrt{(1 - \lambda t)}$. In Eqs (10) and (11), $\beta = (\lambda/a)$ and $M = (\sigma B^2 / a \rho)^{1/2}$ are respectively

the unsteadiness parameter and the magnetic parameter characterizing the strength of the imposed magnetic field.

The appropriate boundary conditions are obtained from Eqs (5) and (6) as

$$f(0) = 0, \quad f'(0) = \alpha + \delta f''(0), \quad f'(\infty) = 1, \quad (12)$$

$$h(0) = 1, \quad h(\infty) = 0, \quad (13)$$

here $\delta = L(av)^{1/2}$ is the dimensionless velocity slip parameter and $\alpha = (c/a)$ is the velocity ratio parameter. It is worth mentioning that the non-dimensional velocity slip parameter (δ) is always positive.

The non-dimensional velocity components is be introduced from the Eq (8) as

$$u^* = u \sqrt{\frac{(1 - \lambda t)}{av}} = \xi f'(\eta) + \alpha L h(\eta), \quad (14)$$

$$w^* = w \sqrt{\frac{(1 - \lambda t)}{av}} = -2f(\eta), \quad (15)$$

where

$$\xi = x \left(\frac{a}{v(1 - \lambda t)} \right)^{1/2} \quad \text{and} \quad L = l \left(\frac{a}{v(1 - \lambda t)} \right)^{1/2}. \quad (16)$$

The dimensionless wall shear stress τ is then given by

$$\tau = \xi f''(0) + \alpha L h'(0). \quad (17)$$

3 Heat transfer

The unsteady heat equation for a fluid with viscous and ohmic heating and variable thermal conductivity is given by (see Chiam [25])

$$\frac{\partial T}{\partial t} + \rho c_p \left(u \frac{\partial T}{\partial x} + w \frac{\partial T}{\partial z} \right) = \frac{\partial}{\partial z} \left(\kappa(T) \frac{\partial T}{\partial z} \right) + \mu \left(\frac{\partial u}{\partial z} \right)^2 + \sigma B_0^2 (u - U)^2 - \frac{\partial q_r}{\partial z}, \quad (18)$$

where $\kappa(T)$, c_p and q_r are the temperature dependent thermal conductivity, the specific heat at constant pressure and the radiative heat flux of the fluid, respectively. The second term on the right hand side of Eq (18) represents the viscous dissipation in the flow; the third term stands for the dissipation of the magnetic energy in the form of Joule heating (Shercliff [26]) while the last term is due to the thermal radiation. Here, the temperature dependent thermal conductivity is written in the form (see Chiam [25])

$$\kappa(T) = \kappa_\infty \left[1 + \frac{\epsilon}{\Delta T} \right], \quad (19)$$

where κ_∞ denotes the conductivity of the fluid away from the surface, $\Delta T = T_w - T_\infty$, T_∞ and T_w are free stream temperature and the sheet temperature. ϵ is a small parameter. Substituting Eq (19) into Eq (18), gives

$$\frac{\partial T}{\partial t} + \rho c_p u \frac{\partial T}{\partial x} + \left(\rho c_p w - \frac{\kappa_\infty \epsilon}{\Delta T} \frac{\partial T}{\partial z} \right) \frac{\partial T}{\partial z} = \kappa(T) \frac{\partial^2 T}{\partial z^2} + \mu \left(\frac{\partial u}{\partial z} \right)^2 + \sigma B_0^2 (u - U)^2 - \frac{\partial q_r}{\partial z}, \quad (20)$$

where the radiation heat flux q_r is defined as

$$q_r = -\frac{4\sigma^*}{3k^*} \frac{\partial T^4}{\partial z}, \quad (21)$$

where k^* is the Rosseland mean absorption coefficient and σ^* is denoted as the Stefan-Boltzmann constant. Here, Taylor series expansion is used to expand the temperature variation T^4 about T_∞ , and on neglecting higher order terms we obtain, $T^4 \cong 4T_\infty^3 T - 3T_\infty^4$. [Eq \(20\)](#) becomes

$$\frac{\partial T}{\partial t} + \rho c_p u \frac{\partial T}{\partial x} + \left(\rho c_p w - \frac{\kappa_\infty \epsilon}{\Delta T} \frac{\partial T}{\partial z} \right) \frac{\partial T}{\partial z} = \left(\kappa(T) + \frac{16\sigma^*}{3k^*} \right) \frac{\partial^2 T}{\partial z^2} + \mu \left(\frac{\partial u}{\partial z} \right)^2 + \sigma B_0^2 (u - U)^2. \quad (22)$$

The thermal boundary conditions may vary depending on the different types of heating processes under consideration. In this study, prescribed surface temperature and prescribed wall heat flux conditions are considered as two different examples of heating processes.

3.1 Case 1: Prescribed Surface Temperature (PST)

We assume that the prescribed wall temperature is a quadratic function in x (see Mahapatra and Nanday [\[17\]](#)) given by,

$$T_w = T_\infty + A(x/l_1)^2 (1 - \lambda t)^{-3/2} \quad \text{at} \quad z = 0, \quad (23)$$

$$T \rightarrow T_\infty \quad \text{as} \quad z \rightarrow \infty, \quad (24)$$

where A is a constant, T_w is the variable wall temperature and l_1 is a reference length. The dimensionless temperature θ is defined as

$$\theta = \frac{T - T_\infty}{T_w - T_\infty}. \quad (25)$$

Substituting Eqs (23) and (25) into [Eq \(22\)](#), we get

$$(1 + \epsilon\theta + N_r)\theta'' + \epsilon\theta'^2 + Pr[2f\theta' - 2(f' + \alpha RLh)\theta + E_c(f'' + \alpha RLh')^2 + E_c M^2 (f' - 1 + \alpha RLh)^2 - \frac{\beta}{2}(\eta\theta' + 3\theta)] = 0, \quad (26)$$

where N_r, E_c and Pr denote the radiation parameter, Eckert and Prandtl numbers, respectively. We defined these physical parameters as follows:

$$N_r = \frac{16\sigma^* T_\infty^3}{3\kappa_\infty k^*}, \quad P_r = \frac{\rho c_p}{\kappa_\infty}, \quad E_c = \frac{a^2 l_1^2}{A_0 c_p}, \quad R = \frac{1}{\xi} \quad A = A_0 / \sqrt{1 - \lambda t}, \quad (27)$$

with boundary conditions

$$\theta(0) = 1, \quad \theta(\infty) = 0. \quad (28)$$

3.2 Case 2: Prescribed Wall Heat Flux (PHF)

The heat flux q_w at the surface is assumed to vary as the square of the distance as follows (see Mahapatra and Nanday [\[17\]](#)):

$$-\kappa_\infty \frac{\partial T}{\partial z} = q_w = D(x/l_1)^2 (1 - \lambda t)^{-3/2} \quad \text{at} \quad z = 0, \quad (29)$$

$$T \rightarrow T_\infty \quad \text{as} \quad z \rightarrow \infty, \quad (30)$$

where D is a constant. Here we set

$$T - T_\infty = \frac{D}{\kappa_\infty} \sqrt{\frac{v}{a}} (x/l_1)^2 (1 - \lambda t)^{-3/2} g(\eta), \quad (31)$$

so that [Eq \(22\)](#) is transformed into the equation

$$\begin{aligned} (1 + \epsilon g + N_r)g'' + \epsilon g'^2 + Pr[2fg' - 2(f' + \alpha RLh)g + E_c(f'' + \alpha RLh')^2 \\ + E_c M^2(f' - 1 + \alpha RLh)^2 - \frac{\beta}{2}(\eta g' + 3g)] = 0, \end{aligned} \quad (32)$$

with boundary conditions

$$g'(0) = -1, \quad g(\infty) = 0, \quad (33)$$

where the Eckert number $E_c = \frac{\kappa_\infty a^2 l_1^2 \sqrt{a/v}}{D_0 c_p}$ and $D = D_0/(1 - \lambda t)^{1/2}$. [Eq \(32\)](#) has exactly the same form as [Eq \(26\)](#) but with a different first boundary condition.

4 Method of Solution

Eqs [\(10\)](#), [\(11\)](#) and [\(26\)](#) were solved using the successive relaxation method (SRM), Motsa [\[27\]](#). The SRM is an iterative procedure that works in a similar fashion to the Gauss-Seidel method for algebraic equations. In this case the technique is used to linearize and decouple a system of differential equations. Further details of the rules of the SRM can be found in [\[28, 29\]](#).

The linear terms in each equation are evaluated at the current iteration level $r + 1$ and the non-linear terms are known from the previous iteration level r . The linearized form of Eqs [\(10\)](#), [\(11\)](#) and [\(26\)](#) are

$$f'''_{r+1} + a_{1,r} f''_{r+1} + a_{2,r} f'_{r+1} = R_{1,r}, \quad (34)$$

$$h''_{r+1} + b_{1,r} h'_{r+1} + b_{2,r} h_{r+1} = R_{2,r}, \quad (35)$$

$$(1 + \epsilon \theta_r + Nr) \theta''_{r+1} + c_{r,1} \theta'_{r+1} + c_{r,2} \theta_{r+1} = R_{3,r}, \quad (36)$$

where

$$\begin{aligned} a_{1,r} &= 2f_r - \frac{\beta}{2}\eta, \quad a_{2,r} = \beta + M^2 - f'_r, \\ R_{1,r} &= -[f'^2_r + M^2 + 1 + \beta], \\ b_{1,r} &= 2f_r - \frac{\beta}{2}\eta, \quad b_{2,r} = -[f'_r + M^2 + \beta], \quad R_{2,r} = 0, \\ c_{1,r} &= 2\epsilon \theta'_r + 2Pr f_r - \frac{Pr\beta}{2}\eta, \quad c_{2,r} = \epsilon \theta''_r - 2Pr(f'_{r+1} + \alpha RLh)^2 - \frac{3Pr\beta}{2}, \\ R_{3,r} &= Pr E_c [(f''_r + \alpha RLh'_r)^2 + M^2(f'_r + \alpha RLh_r)^2] - \epsilon \theta''_r \theta_r - \epsilon \theta'^2_r. \end{aligned}$$

It must be noted that Eqs [\(34\)](#)–[\(36\)](#) are linear and decoupled and can thus be solved sequentially to obtain the quantities $f(\eta)$, $h(\eta)$ and $\theta(\eta)$. We opted in this study to use the Chebyshev spectral collocation method to discretize in η and finite differences with central differencing to discretize in ξ . Starting from initial guesses $f_0(\eta)$, $\theta_0(\eta)$ and $\phi_0(\eta)$, Eqs [\(34\)](#)–[\(36\)](#) were solved

iteratively until the approximate solutions converged to within a certain prescribed tolerance level.

Similarly, for the PHF case, Eqs (10), (11) and (32) take the form

$$f'''_{r+1} + a_{1,r}f''_{r+1} + a_{2,r}f'_{r+1} = R_{1,r}, \quad (37)$$

$$h''_{r+1} + b_{1,r}h'_{r+1} + b_{2,r}h_{r+1} = R_{2,r}, \quad (38)$$

$$(1 + \epsilon g_r + Nr)g''_{r+1} + c_{r,1}g'_{r+1} + c_{2,r}g_{r+1} = R_{3,r}, \quad (39)$$

where

$$\begin{aligned} a_{1,r} &= 2f_r - \frac{\beta \eta}{2}, \quad a_{2,r} = \beta + M^2 - f'_r, \\ R_{1,r} &= -[f'^2 + M^2 + 1 + \beta], \\ b_{1,r} &= 2f_r - \frac{\beta \eta}{2}, \quad b_{2,r} = -[f'_r + M^2 + \beta], \quad R_{2,r} = 0, \\ c_{1,r} &= 2\epsilon g'_r + 2Pr f_r - \frac{Pr\beta \eta}{2}, \quad c_{2,r} = \epsilon g''_r - 2Pr(f'_{r+1} + \alpha R L h)^2 - \frac{3Pr \beta}{2}, \\ R_{3,r} &= Pr E_c [(f''_r + \alpha R L h'_r)^2 + M^2(f'_r + \alpha R L h_r)^2] - \epsilon g''_r g_r - \epsilon g'^2_r. \end{aligned}$$

5 Results and Discussion

The analysis of the results presented here relate to a decelerating shrinking sheet only (i.e., $\beta \leq 0$) following Fang et al.[30], Rohini et al.[31] and Nandy et al.[32]. We have compared the local skin friction coefficients $f'(0)$ and $h'(0)$ for various values of the parameter α with previously published data (Wang [15], Rahimpour et al. [33] and Mahapatra and Nandy [17]). The comparisons are shown in Table 1 where we observe an very good agreement to the results in the literature thus validating the current numerical results.

The phenomena of heat transfer is studied with respect to the numerical values of the physical parameters namely, (a) the wall temperature gradient $-\theta'(0)$ in the PST case and (b) the

Table 1. Comparison table of the values of $f'(0)$ and $h'(0)$ when $M = 0$ with recent literature.

α	$f'(0)$				$h'(0)$			
	Wang [15]	Rahimpour et al. [33]	Mahapatra and Nanday [17]	Present Results	Wang [15]	Rahimpour et al. [33]	Mahapatra and Nanday [17]	Present Results
-0.95	0.9469	0.946815	0.946893	0.946897	0.26845	0.268450	0.268457	0.268458
-0.75	1.35284	1.352850	1.352841	1.352854	-0.22079	-0.220789	-0.220795	-0.220785
-0.50	1.49001	1.490004	1.352841	1.352852	-0.53237	-0.532371	-0.532374	-0.532379
-0.25	1.45664	1.456599	1.456641	1.456648	-0.75639	-0.756390	-0.756380	-0.756376
0.0	1.31193	1.311938	1.311942	1.311950	-0.93873	-0.938732	-0.938731	-0.938745
0.1	1.22911	1.229113	1.229111	1.229117	-1.00400	-1.004026	-1.004031	-1.004032
0.2	1.13374	1.133743	1.133750	1.133757	-1.06590	-1.065933	-1.065951	-1.065946
0.5	0.78032	0.780323	0.780327	0.780332	-1.23550	-1.235451	-1.235460	-1.235454
1.0	0	0	0	0	-1.47930	-1.479337	-1.479341	-1.479332
2.0	-2.13107	-2.131069	-2.131068	-2.131075	-1.88000	-1.879949	-1.879956	-1.879945
5.0	-11.8022	-11.802214	-11.802202	-11.802213	-2.76170	-2.761724	-2.761702	-2.76167

doi:10.1371/journal.pone.0138355.t001

Table 2. Wall temperature gradient $|\theta'(0)|$ for the PST case taking $Pr = 0.72, R = 1, \beta = -0.25, L = 1, E_c = 1$ and $Nr = 2.0$.

ϵ	α	$M = 0.0$	$M = 0.5$	$M = 1.0$
0.0	-0.9	0.470476	0.515791	0.639041
	-0.3	0.469680	0.497224	0.575271
	-0.1	0.389930	0.402194	0.436688
0.1	-0.9	0.435015	0.477871	0.594412
	-0.3	0.434487	0.460699	0.535030
	-0.1	0.358828	0.370508	0.403393
0.2	-0.9	0.403350	0.443995	0.554504
	-0.3	0.403116	0.428120	0.499084
	-0.1	0.331167	0.342317	0.373743

doi:10.1371/journal.pone.0138355.t002

wall temperature $|g(0)|$ in the PHF case. Tables 2 and 3 show that the wall temperature gradient $|\theta'(0)|$ in the PST case and the wall temperature $|g(0)|$ in the PHF case increases with increasing M when α and ϵ are fixed. The temperature gradient in the PST case and the wall temperature in the PHF case decrease with increases in the thermal conductivity parameter ϵ . We also observe that $|\theta'(0)|$ and $|g(0)|$ decrease as α increases in both the PST and the PHF cases.

Fig 2 depicts the variation of the skin friction coefficients $f''(0)$ and $h'(0)$ with $\alpha < 0$ (shrinking sheet) and $\alpha > 0$ (stretching sheet) for different values of the magnetic parameter M . Here solid and dashed lines represent the trajectories of $f''(0)$ and $h'(0)$, respectively. Our numerical results reveal that without a magnet (i.e., $M = 0$), Eqs (14) and (15) have unique solutions when $\alpha \geq -1$ and no similarity solution exists for $\alpha < -1$. It is observed that the similarity solution exists up to a critical value $\alpha = \alpha_c (< 0)$, (say) beyond which a solution based on the boundary layer approximations does not exist as the boundary layer separates from the surface. From a physical point of view, a steady solution is not possible unless additional fluid from the stagnation-point is added to the free stream. A steady solution is possible only when ratio of the free stream velocity and shrinking velocity is less than a certain numerical value which again depends on the magnetic field parameter (M). The results show that when M increases, the range of α where similarity solutions exist gradually increases. When $\alpha = 1$, we find that $f''(0) = 0$ because $f(\eta) = \eta$ is the solution of Eq (14) subject to the boundary conditions Eq (16). The results show that when $f''(0) \geq 0$, for a given value of α , $f''(0)$ increases with M . For a shrinking surface, the $h'(0)$ orbits intersect the α -axis but this is not the case for flow over a stretching

Table 3. Wall temperature gradient $|g(0)|$ for the PHF case taking $Pr = 0.72, R = 1, \beta = -0.25, L = 1, E_c = 1$ and $Nr = 2.0$.

ϵ	α	$M = 0.0$	$M = 0.5$	$M = 1.0$
0.0	-0.9	0.649572	0.681891	0.764965
	-0.3	0.593890	0.618274	0.686943
	-0.1	0.505823	0.517244	0.549463
0.1	-0.9	0.616233	0.648325	0.731028
	-0.3	0.555240	0.579129	0.646413
	-0.1	0.467061	0.478199	0.509608
0.2	-0.9	0.585066	0.616894	0.699120
	-0.3	0.519071	0.542448	0.608305
	-0.1	0.430932	0.441781	0.472366

doi:10.1371/journal.pone.0138355.t003

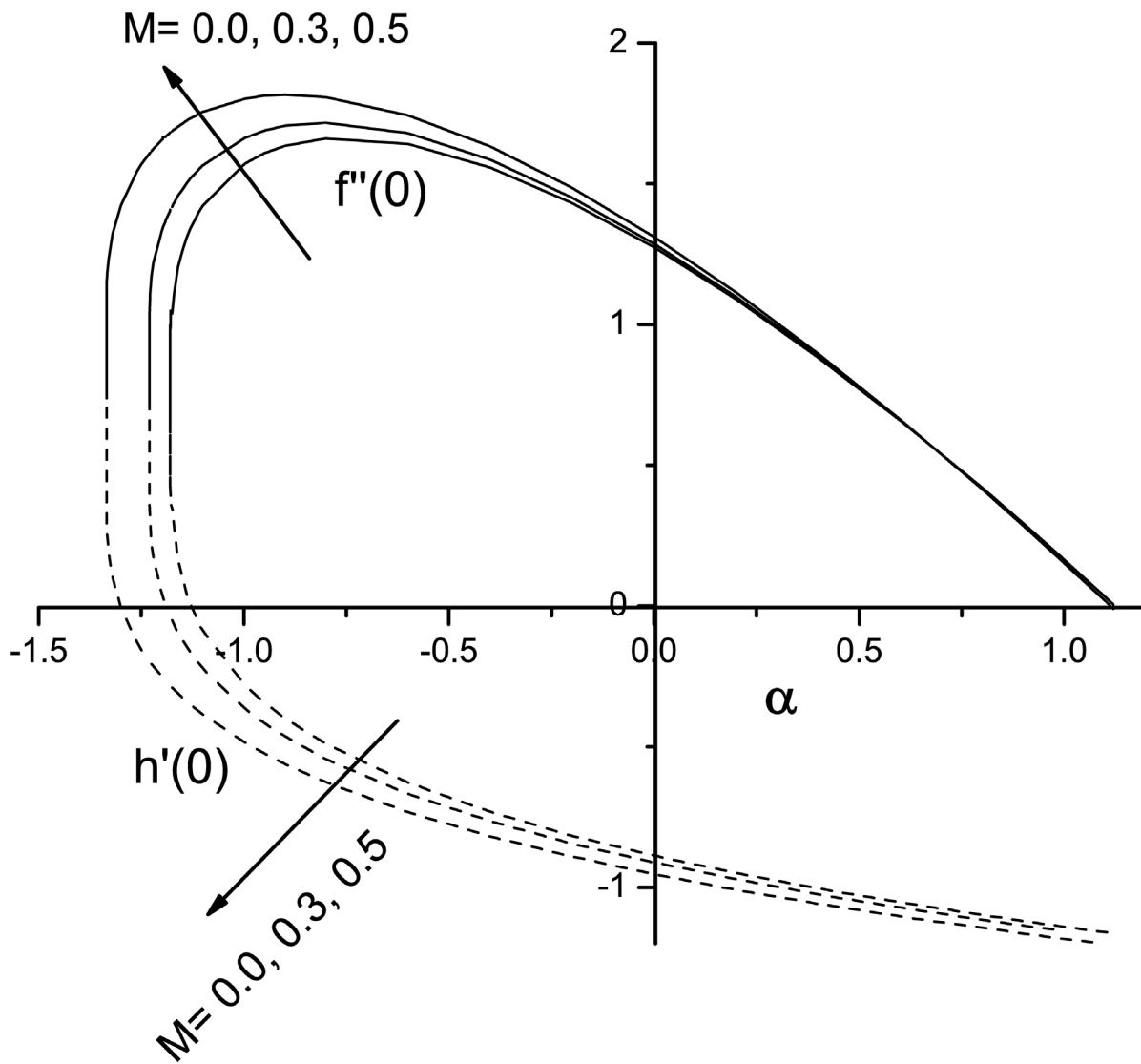


Fig 2. Initial values $F'(0)$ and $h'(0)$ versus α and M .

doi:10.1371/journal.pone.0138355.g002

sheet. For a given value of M , the size of $h'(0)$ decreases with increases in $|\alpha|$. Also, for any given α , $|h'(0)|$ increases with M .

We note that for a stretching sheet α is positive and for a shrinking sheet α is negative while $\alpha = 0$ represents Hiemenz flow. Figs 3 and 4 show the effect of α on the vertical velocity components $f(\eta)$ and $h(\eta)$. We observe that $f(\eta)$ increases with increases in α while the value of $h(\eta)$ decreases with increases in the values of α .

Fig 5 displays the effect of α on the temperature profiles $\theta(\eta)$ (for PST case). Here the temperature profiles decrease with an increase in α . Figs 6 and 7 show the effect of M on $f(\eta)$ and non-alignment variable $h(\eta)$ with respect to η , respectively. It is clear that $f(\eta)$ increases with increasing values of the magnetic parameter M and $h(\eta)$ decreases with M . We can conclude from the above results is that for shrinking sheet, the effect of non-alignment becomes less pronounced with increasing M .

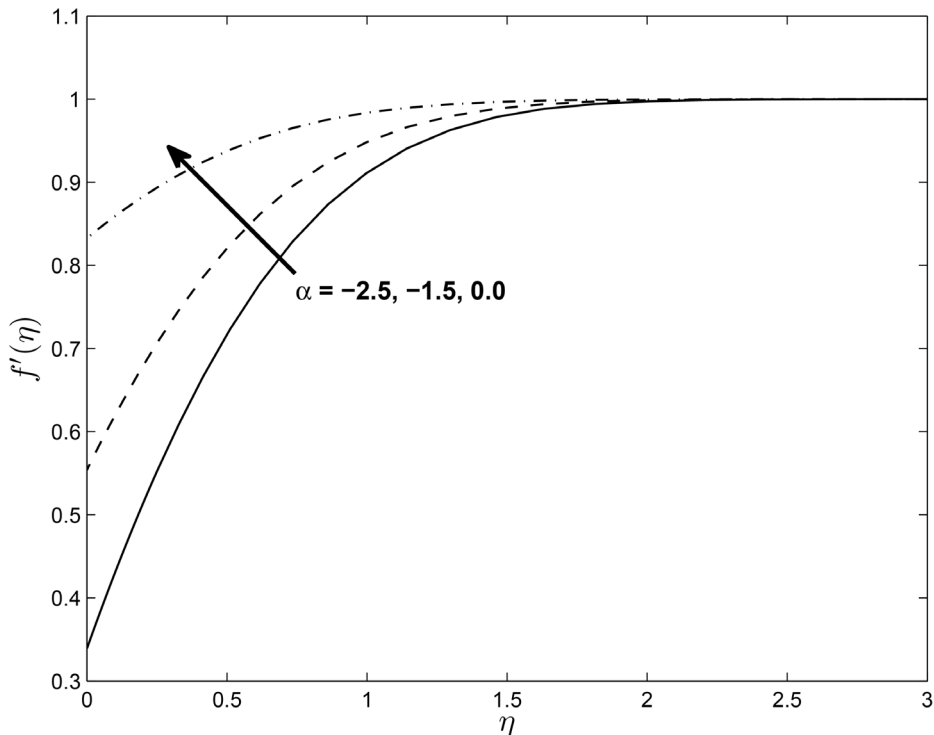


Fig 3. Effect of α on velocity profiles $f'(\eta)$ for $M = 0.1, \delta = 0.2, \beta = -0.25, Pr = 0.72, Nr = 0.2, Ec = 1.0, R = 1.0$ and $\epsilon = 0.5$.

doi:10.1371/journal.pone.0138355.g003

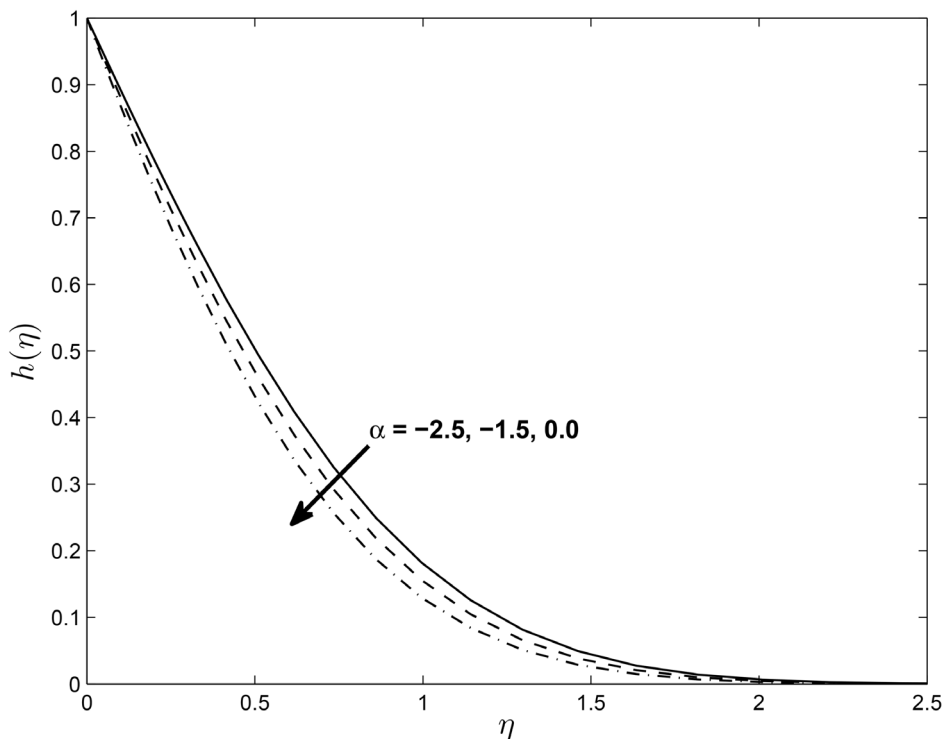


Fig 4. Effect of α on velocity profiles $h(\eta)$ for $M = 0.1, \delta = 0.2, \beta = -0.25, Pr = 0.72, Nr = 0.2, Ec = 1.0, R = 1.0$ and $\epsilon = 0.5$.

doi:10.1371/journal.pone.0138355.g004

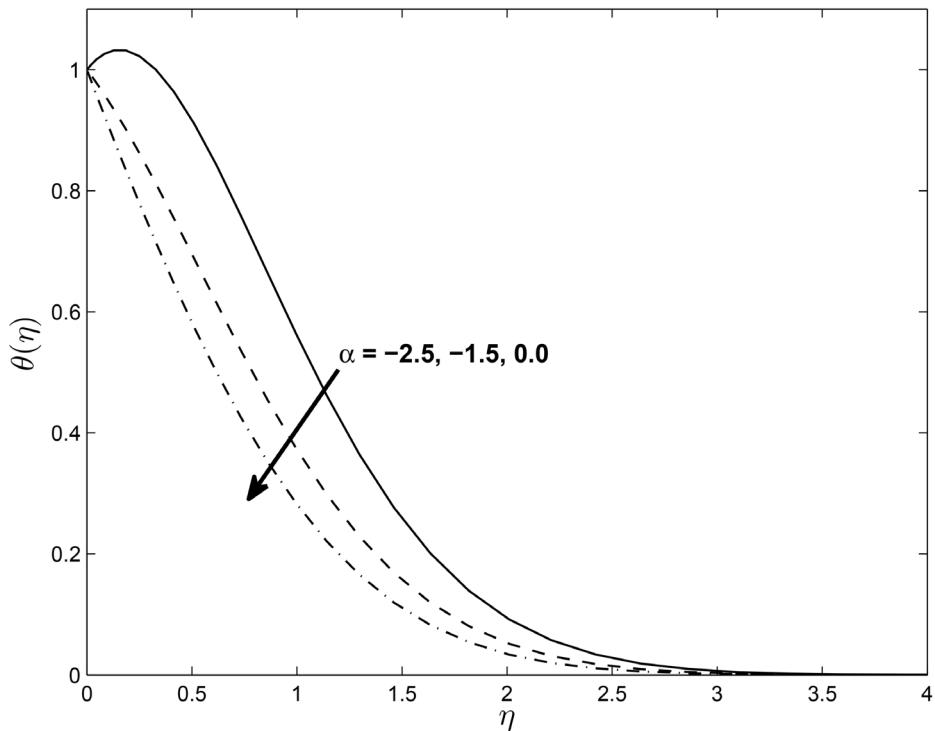


Fig 5. Effect of α on temperature profile for $M = 0.1$, $\delta = 0.2$, $\beta = -0.25$, $Pr = 0.72$, $Nr = 0.2$, $Ec = 1.0$, $R = 1.0$, $L = 1.0$ and $\epsilon = 0.5$.

doi:10.1371/journal.pone.0138355.g005

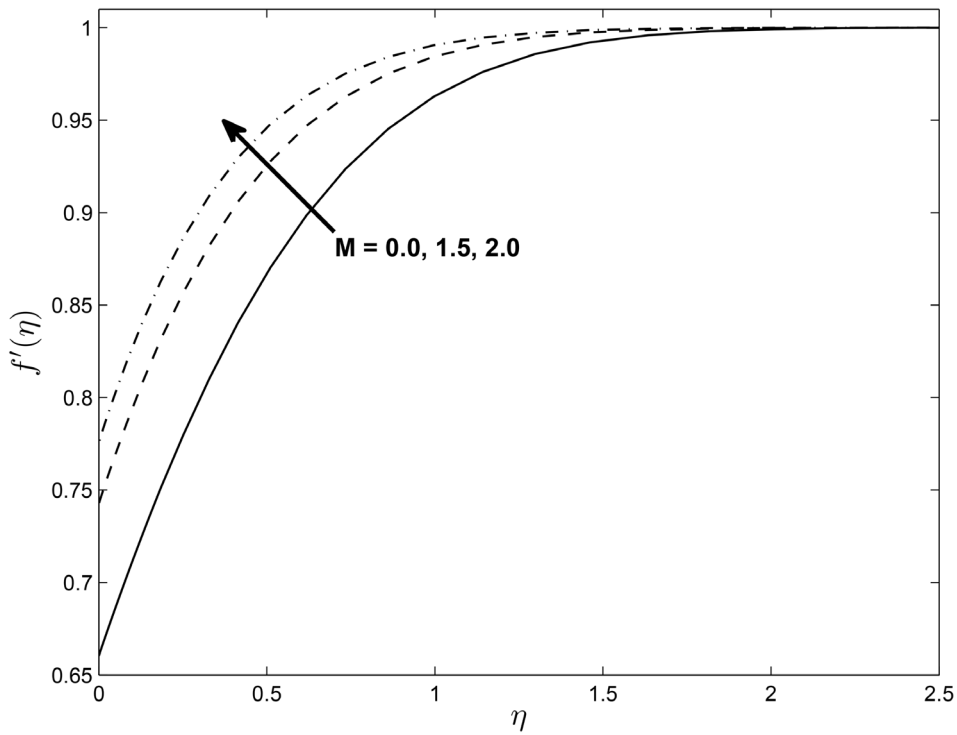


Fig 6. Effect of magnetic parameter M on velocity profiles $f(\eta)$ for $\delta = 0.2$, $\beta = -0.25$, $\alpha = -0.95$, $Pr = 0.72$, $Nr = 0.2$, $Ec = 1.0$, $R = 1.0$, $L = 1.0$ and $\epsilon = 0.5$.

doi:10.1371/journal.pone.0138355.g006

Figs 8 and 9 show that the temperature profiles decrease monotonically with an increase in the magnetic parameter in both the PST and the PHF cases, respectively. The extent of the reverse circular flow above the sheet decreases with increases in M . This is a consequence of the fact that the temperature field given by Eq (18) is influenced by the advection of the fluid velocity above the sheet. Figs 10 and 11 exhibit the temperature profiles for different values of thermal conductivity parameter ϵ where the other parameters are fixed for both the PST and PHF cases, respectively. The temperature profiles increase with an increase in the thermal conductivity parameter due to increases in the thermal boundary layer thickness in both the PST and PHF cases.

Figs 12 and 13 depict the horizontal velocity profiles $f'(\eta)$ and $h(\eta)$ for different values of the unsteadiness parameter β in the presence of slip at the boundary, respectively. The velocity $f'(\eta)$ decreases with an increase in the unsteadiness parameter β and this implies an accompanying reduction in the thickness of the momentum boundary layer while the opposite trend is observed with $h(\eta)$. We observe that as β increases, the axial boundary layer velocity decreases. In the vicinity of the sheet, the axial fluid velocity decreases while the trend is reversed in the free stream. The parameter β has the effect of reducing the momentum boundary layer thickness for $f'(\eta)$ while enhancing the boundary layer thickness of $h(\eta)$.

Figs 14, 15 and 16 show the effect of δ on the velocity components $f'(\eta)$, $h(\eta)$ and temperature profile $\theta(\eta)$ (for PST case), respectively. It is interesting to note that the velocity profile $f'(\eta)$ increases with increase in values of δ while $h(\eta)$ decreases with the increase in the values of δ . The figure also reveals that the temperature profile $\theta(\eta)$ decreases with the increase in the values of δ . This may be explained in the following way; with slip, there is a difference between the flow velocity near the sheet and the shrinking velocity at the surface. As δ increases the slip velocity increases leading to a decrease in the fluid velocity for $h(\eta)$. But the opposite trend is observed for $f'(\eta)$ because momentum boundary layer become thinner due to increasing value of δ . Fig 16 illustrates the fact that the temperature at any given point increases when the slip velocity δ increases.

Figs 17 and 18 depict the effect of Nr on the temperature profile in PST and PHF cases with keeping other parameters fixed, respectively. The temperature profile in two cases increase with increasing in values of Nr , which in turn increases the thermal boundary layer thickness for both PST and PHF cases. This may due to the fact that increases in the value of Nr causes an increase in the interaction with the thermal boundary layer.

Figs 19 and 20 show the variation in the skin friction coefficient $-f''(0)$ with respect to β . We observe that the skin friction coefficients decrease monotonically with increasing values of β and M in Fig 19 while the opposite is true in the Fig 20 for β and δ . The highest value of the skin friction is reached for smaller values of β .

Figs 21 and 22 display the dimensionless wall heat transfer rates $-\theta'(0)$ as a function of β . We observe that the wall heat transfer rate increases with increasing β , M and δ . The maximum value of the dimensionless wall heat transfer rates is achieved for large values of β .

6 Conclusion

An unsteady MHD axisymmetric stagnation-point flow over a shrinking sheet with temperature dependent thermal conductivity and thermal radiation and a Navier slip was investigated in this paper. The surface was assumed to shrink axisymmetrically in its own plane and the flow was permeated by a uniform magnetic field normal to the surface. The temperature profiles in the two cases of prescribed wall temperature and prescribed surface heat flux was shown to increase with the thermal radiation parameter, which in turn increases the thermal boundary layer thickness for both PST and PHF cases. This may be due to the fact that an

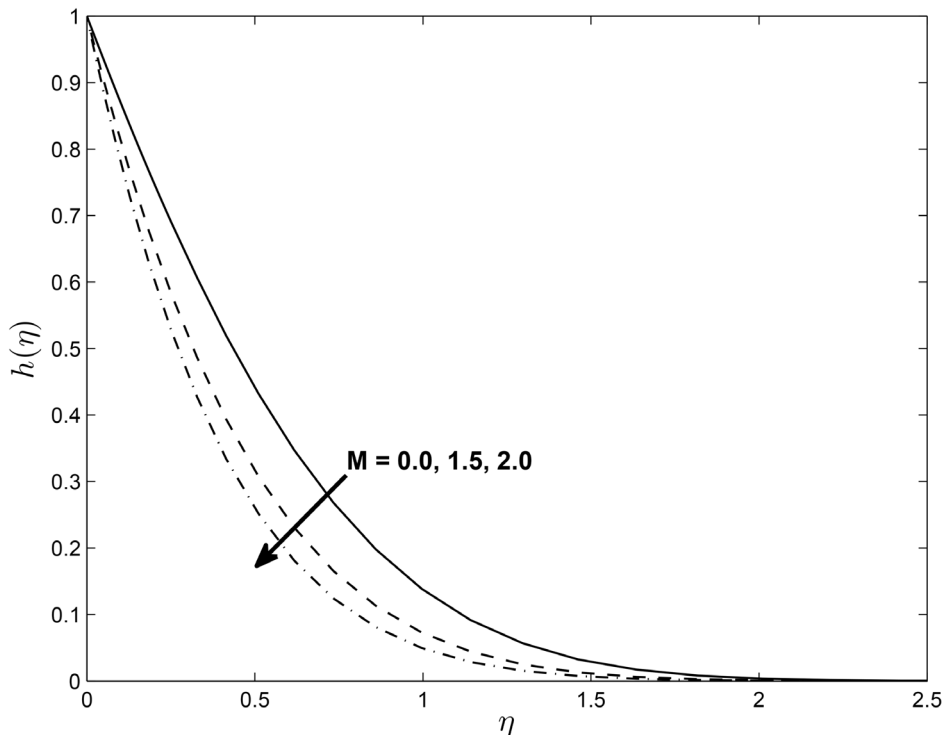


Fig 7. Effect of magnetic parameter M on velocity profiles $h(\eta)$ for $\delta = 0.2, \beta = -0.25, \alpha = -0.95, Pr = 0.72, Nr = 0.2, Ec = 1.0, R = 1.0, L = 1.0$ and $\epsilon = 0.5$.

doi:10.1371/journal.pone.0138355.g007

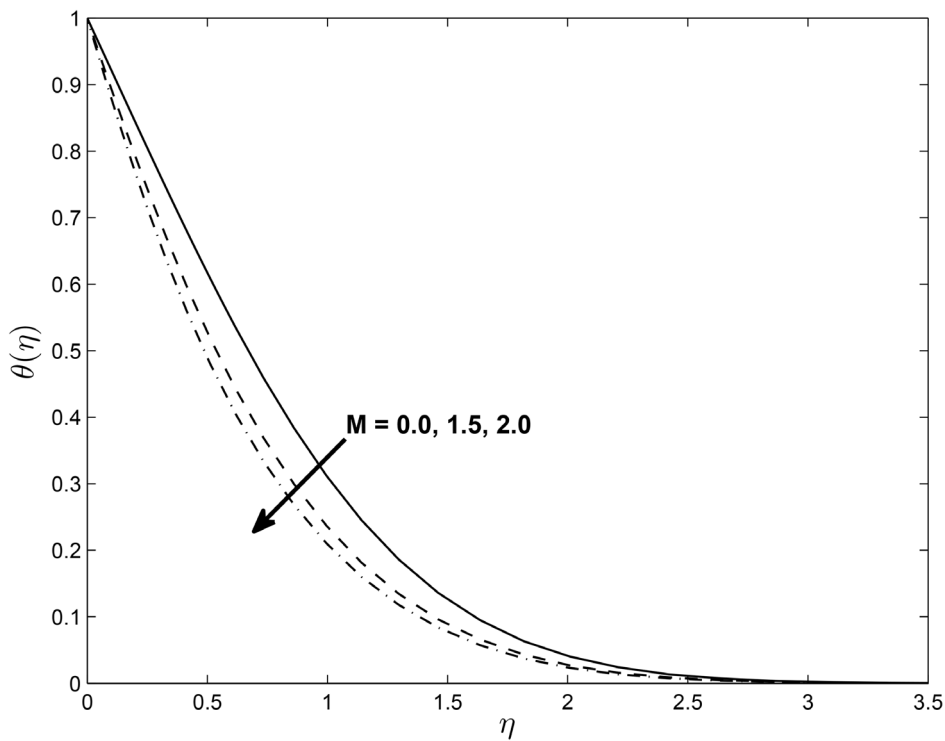


Fig 8. Effects of magnetic parameter M on temperature profiles (PST case) for $\delta = 0.2, \beta = -0.25, \alpha = -0.95, Pr = 0.72, Nr = 0.2, Ec = 1.0, R = 1.0$ and $L = 1.0$.

doi:10.1371/journal.pone.0138355.g008

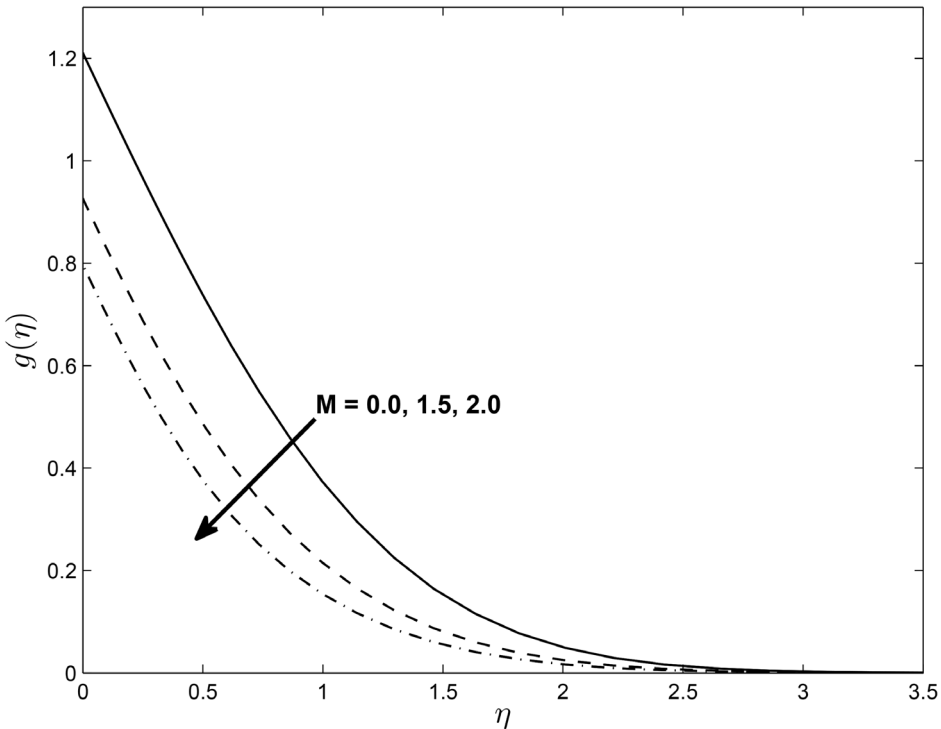


Fig 9. Effects of magnetic parameter M on temperature profiles (PHF case) for $\delta = 0.2$, $\beta = -0.25$, $\alpha = -0.95$, $Pr = 0.72$, $Nr = 0.2$, $Ec = 1.0$, $R = 1.0$ and $L = 1.0$.

doi:10.1371/journal.pone.0138355.g009

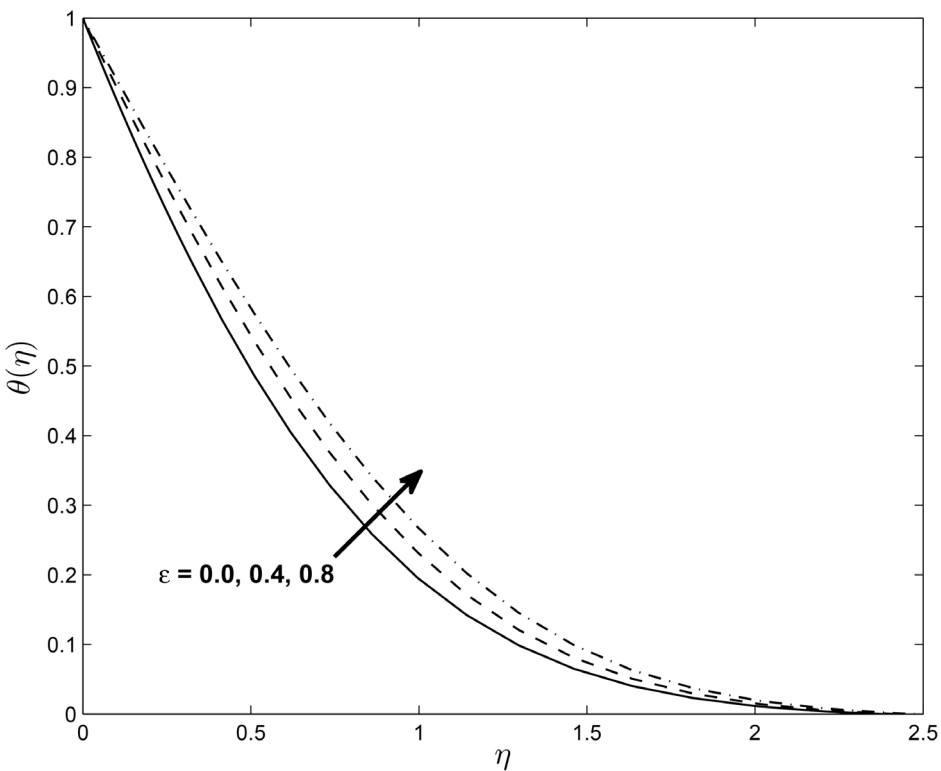


Fig 10. Effects of ϵ on temperature profiles (PST case) for $\delta = 0.2$, $\beta = -0.25$, $\alpha = -0.95$, $Pr = 0.72$, $Nr = 0.2$, $Ec = 1.0$, $R = 1.0$ and $L = 1.0$.

doi:10.1371/journal.pone.0138355.g010

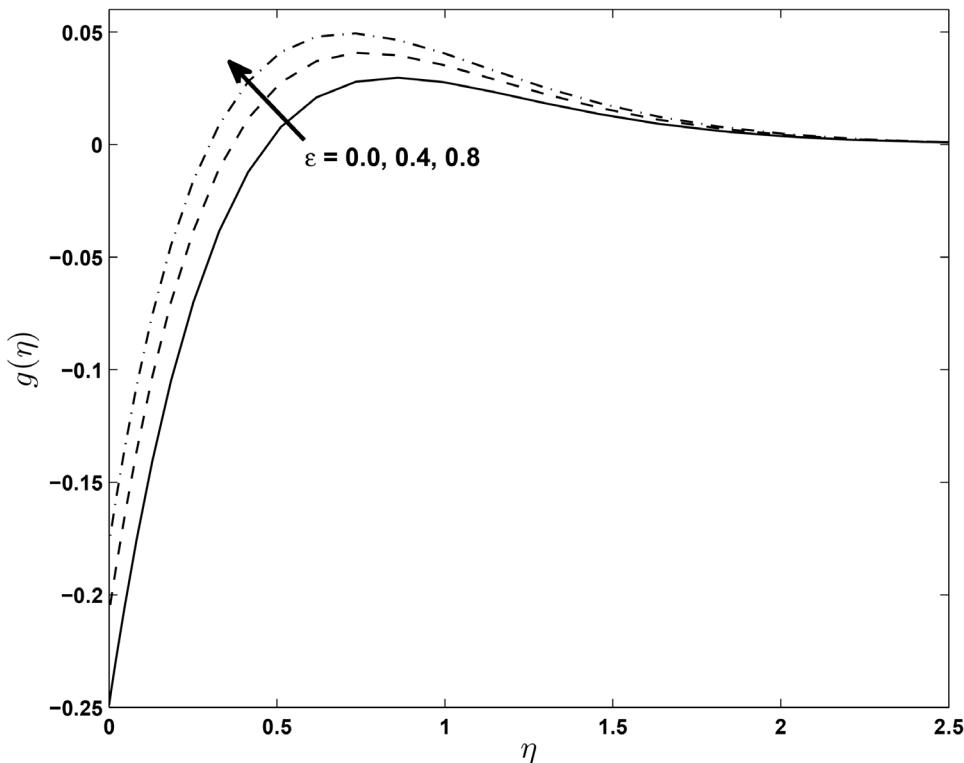


Fig 11. Effects of ϵ on temperature profiles (PHF case) for $\delta = 0.2$, $\beta = -0.25$, $\alpha = -0.95$, $Pr = 0.72$, $Nr = 0.2$, $Ec = 1.0$, $R = 1.0$ and $L = 1.0$.

doi:10.1371/journal.pone.0138355.g011

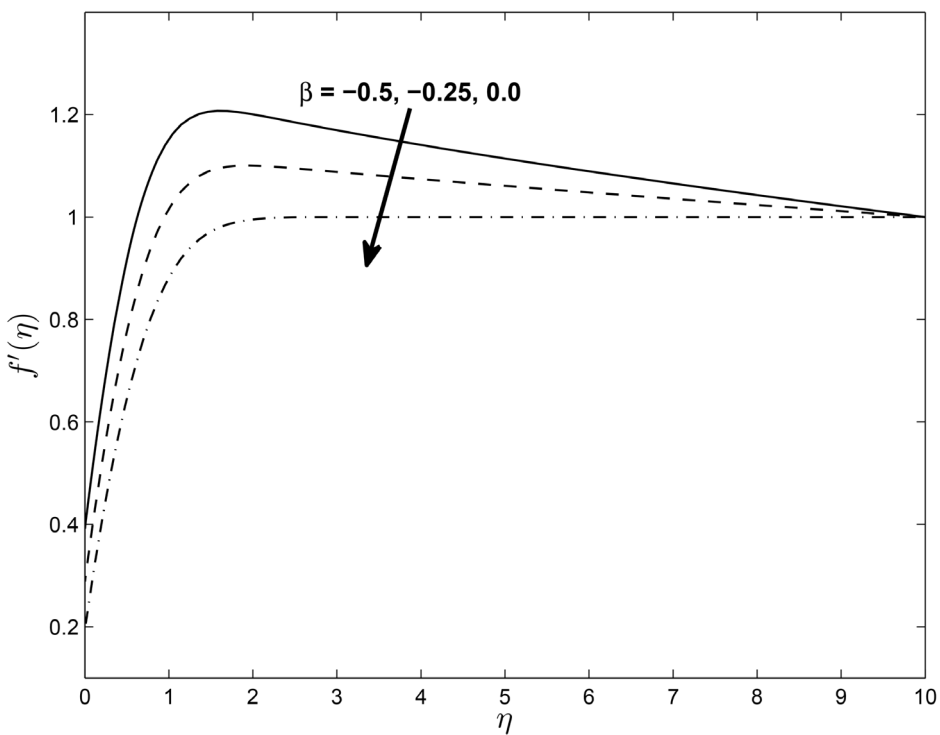


Fig 12. Effect of β on velocity profiles $f'(\eta)$ for $M = 0.1$, $\delta = 0.2$, $\alpha = -0.95$, $Pr = 0.72$, $Nr = 0.2$, $Ec = 1.0$, $R = 1.0$, $L = 1.0$ and $\epsilon = 0.5$.

doi:10.1371/journal.pone.0138355.g012

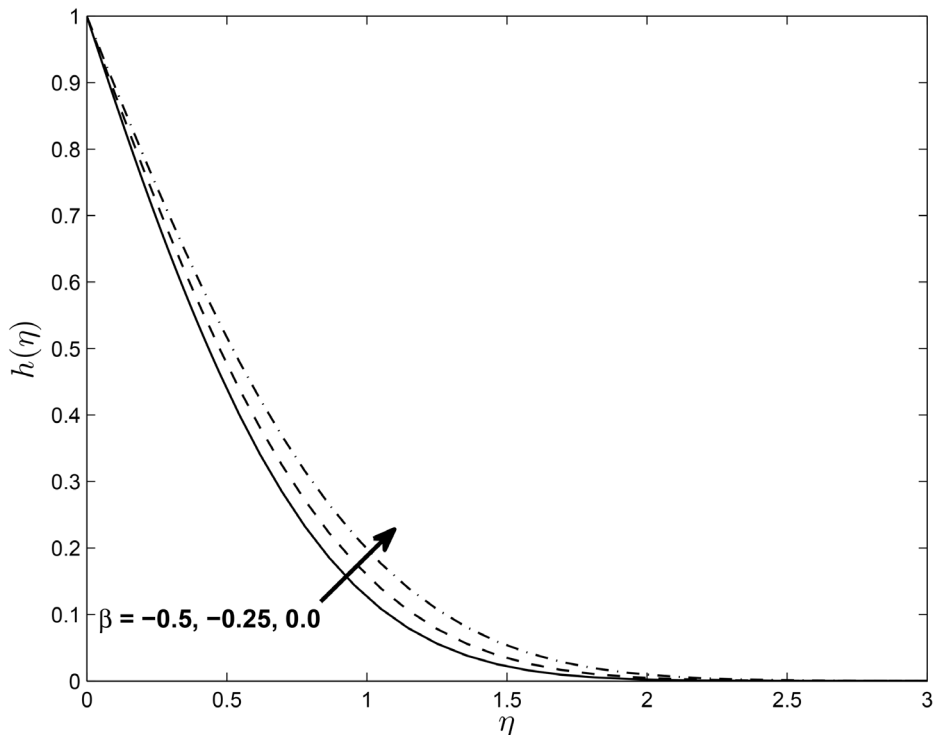


Fig 13. Effect of β on velocity profiles $h(\eta)$ for $M = 0.1$, $\delta = 0.2$, $\alpha = -0.95$, $Pr = 0.72$, $Nr = 0.2$, $Ec = 1.0$, $R = 1.0$, $L = 1.0$ and $\epsilon = 0.5$.

doi:10.1371/journal.pone.0138355.g013

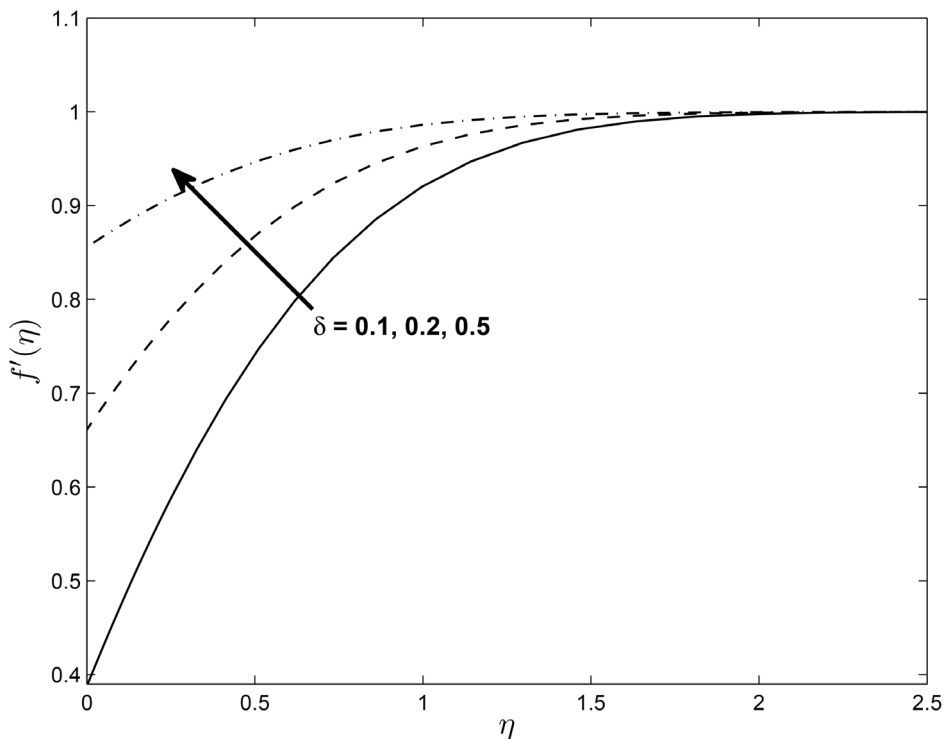


Fig 14. Effect of δ on velocity profiles $f'(\eta)$ for $M = 0.1$, $\beta = -0.25$, $\alpha = -0.95$, $Pr = 0.72$, $Nr = 0.2$, $Ec = 1.0$, $R = 1.0$, $L = 1.0$ and $\epsilon = 0.5$.

doi:10.1371/journal.pone.0138355.g014

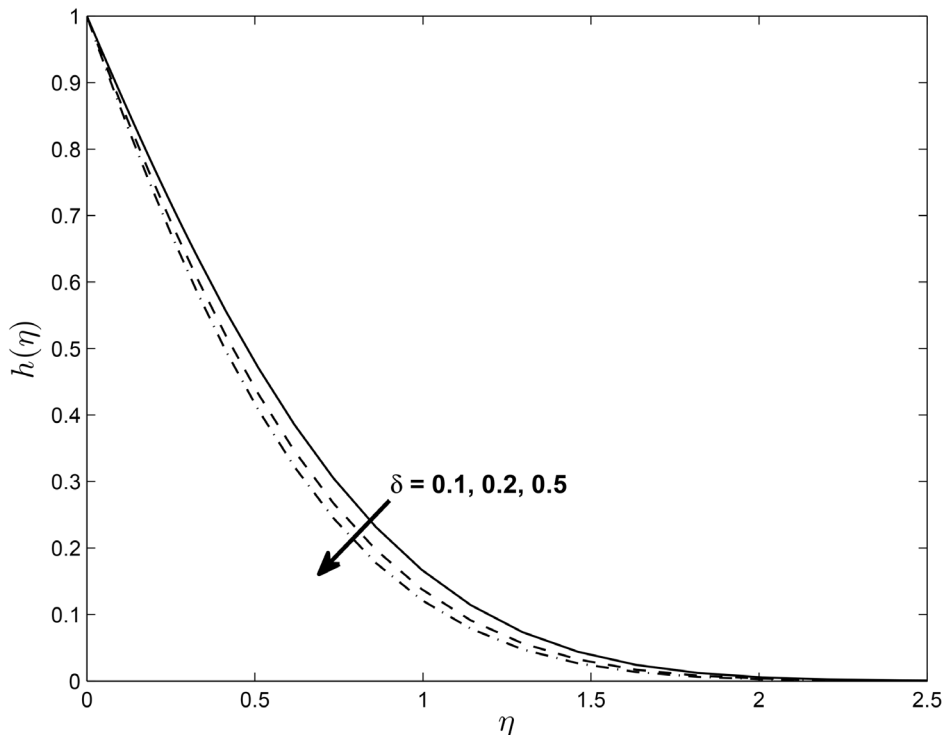


Fig 15. Effect of δ on velocity profiles $h(\eta)$ for $M = 0.1, \beta = -0.25, \alpha = -0.95, Pr = 0.72, Nr = 0.2, Ec = 1.0, R = 1.0, L = 1.0$ and $\epsilon = 0.5$.

doi:10.1371/journal.pone.0138355.g015

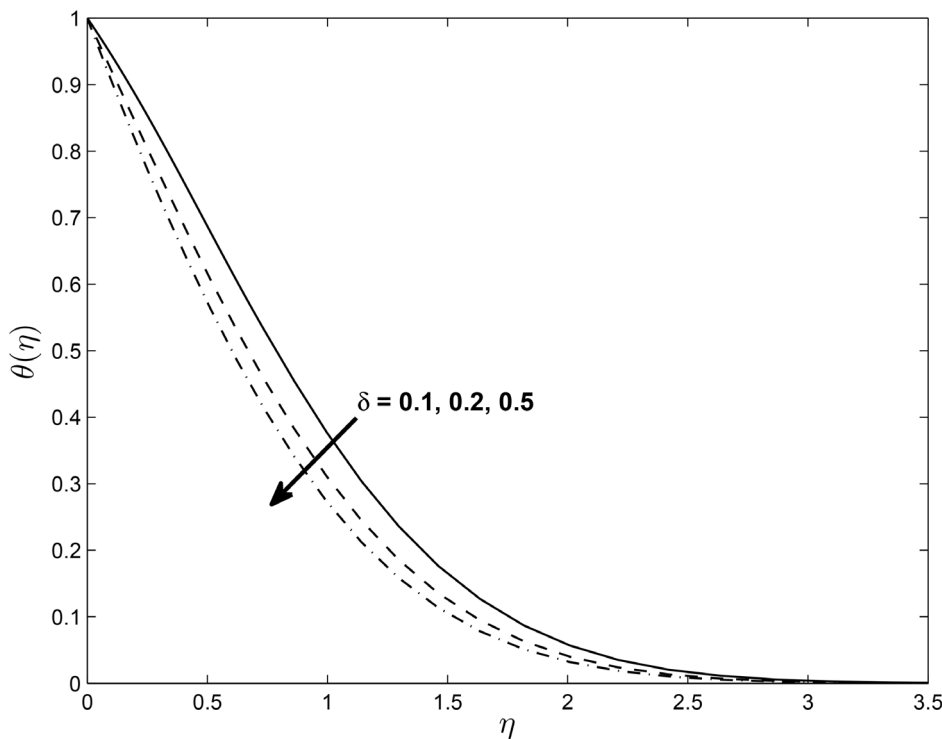


Fig 16. Effect of δ on temperature profile (PST case) for $M = 0.1, \beta = -0.25, \alpha = -0.95, Pr = 0.72, Nr = 0.2, Ec = 1.0, R = 1.0, L = 1.0$ and $\epsilon = 0.5$.

doi:10.1371/journal.pone.0138355.g016

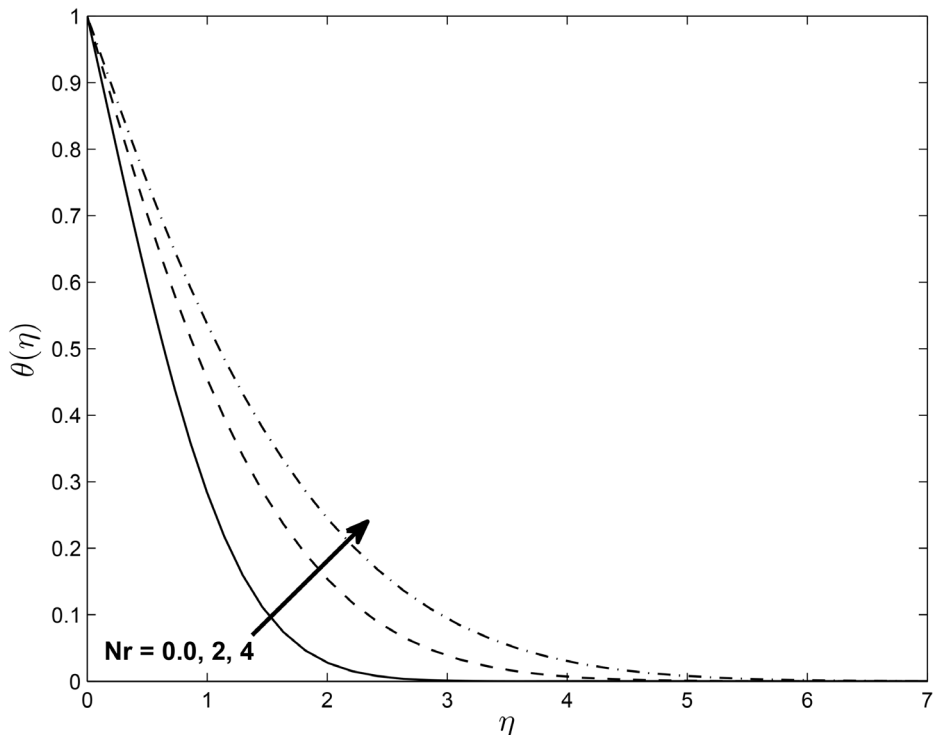


Fig 17. Effects of thermal radiation parameter Nr on temperature profiles $\theta(\eta)$ for $\delta = 0.2$, $Pr = 0.72$, $\beta = -0.25$, $Ec = 1.0$, $\alpha = -0.95$, $M = 0.1$, $R = 1.0$ and $L = 1.0$.

doi:10.1371/journal.pone.0138355.g017

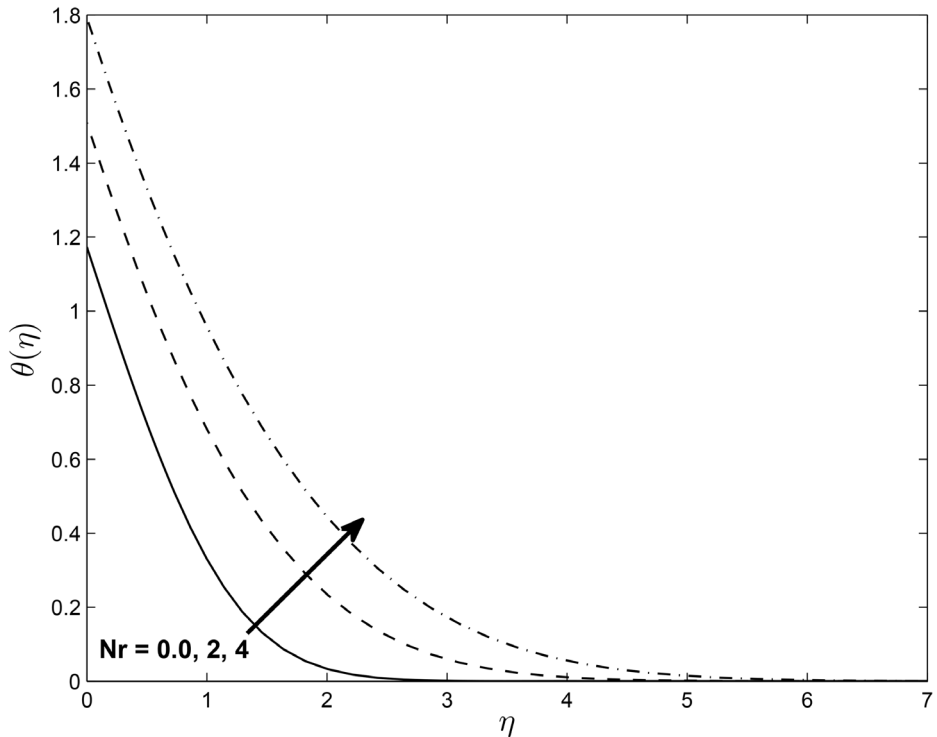


Fig 18. Effects of thermal radiation parameter Nr on temperature profiles $g(\eta)$ for $\delta = 0.2$, $Pr = 0.72$, $\beta = -0.25$, $Ec = 1.0$, $\alpha = -0.95$, $M = 0.1$, $R = 1.0$ and $L = 1.0$.

doi:10.1371/journal.pone.0138355.g018

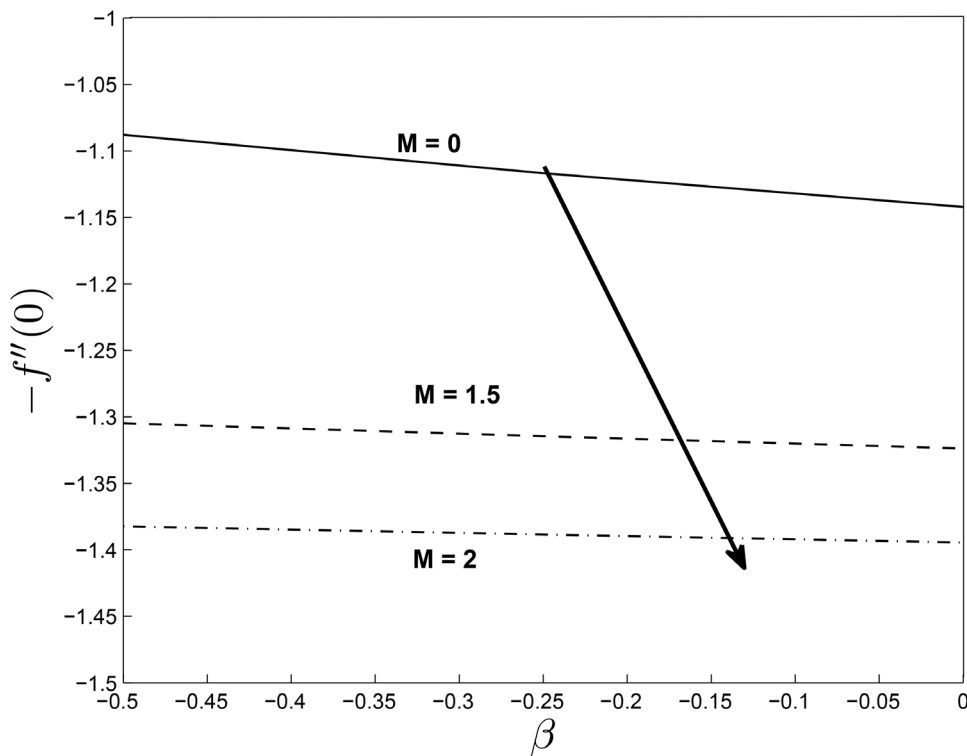


Fig 19. Effect of M on Skin friction coefficients for $\alpha = -0.95$, $Pr = 0.72$, $Nr = 0.2$, $Ec = 1.0$, $R = 1.0$, $L = 1.0$ and $\epsilon = 0.5$.

doi:10.1371/journal.pone.0138355.g019

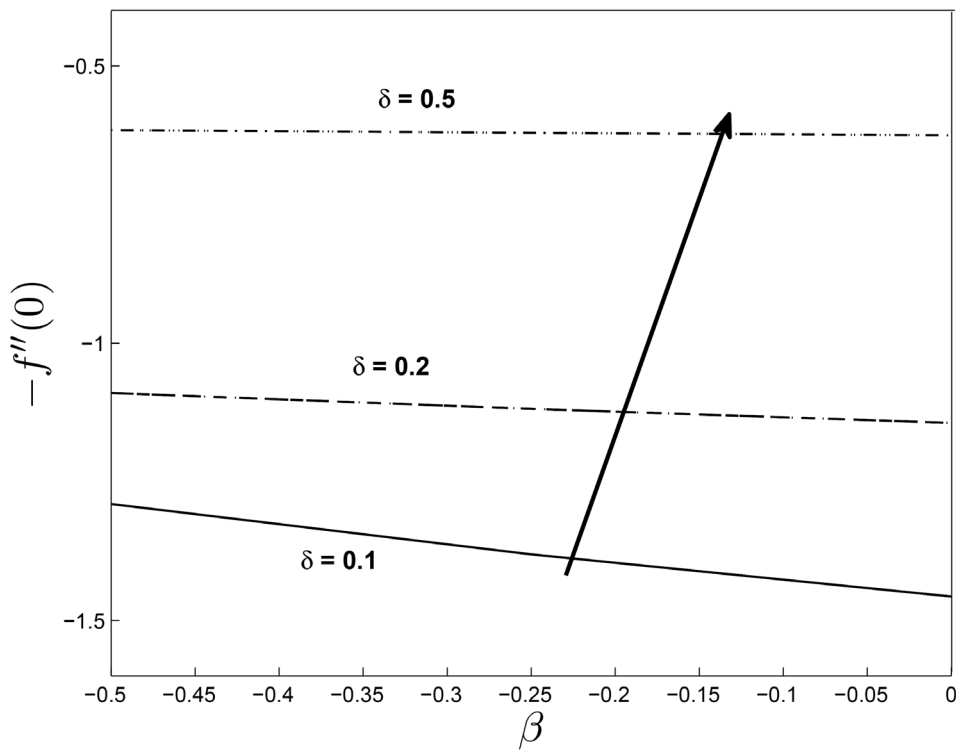


Fig 20. Effect of δ on Skin friction coefficients for $\alpha = -0.95$, $Pr = 0.72$, $Nr = 0.2$, $Ec = 1.0$, $R = 1.0$, $L = 1.0$ and $\epsilon = 0.5$.

doi:10.1371/journal.pone.0138355.g020

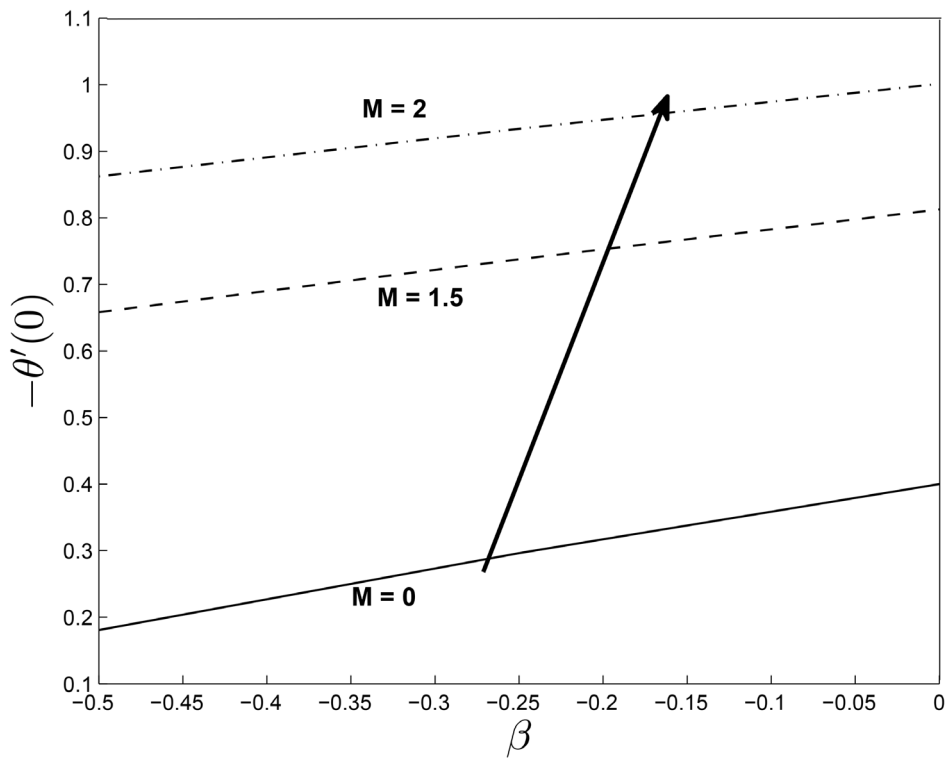


Fig 21. Effect of M on heat transfer coefficients for $\alpha = -0.95, Pr = 0.72, Nr = 0.2, Ec = 1.0, R = 1.0, L = 1.0$ and $\epsilon = 0.5$.

doi:10.1371/journal.pone.0138355.g021

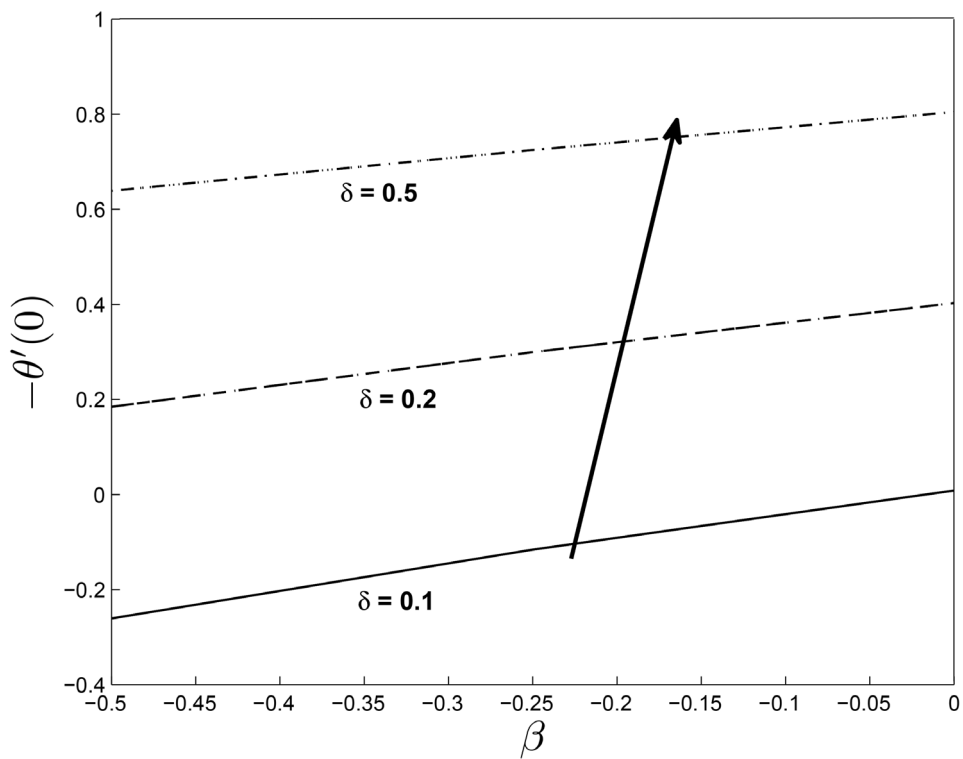


Fig 22. Effect of δ on heat transfer coefficients for $\alpha = -0.95, Pr = 0.72, Nr = 0.2, Ec = 1.0, R = 1.0, L = 1.0$ and $\epsilon = 0.5$.

doi:10.1371/journal.pone.0138355.g022

increase in N , induces a significant interaction between the fluid and the thermal boundary layer. It is clear that $f'(\eta)$ increases with increasing magnetic parameter values M while $h(\eta)$ decreases with the magnetic parameter. It can be concluded that for a shrinking sheet, the effect of non-alignment becomes less pronounced with enhanced magnetic parameter values. When slip occurs, the flow velocity near the sheet is no longer equal to the shrinking velocity at the sheet. Then with an increase in δ such slip velocity increases and consequently fluid velocity decreases for $h(\eta)$ under the slip condition at the boundary.

Acknowledgments

Authors wish to thank the referees for their valuable suggestions. Also, authors are thankful to Dr. Samir Kumar Nandy for his valuable suggestions which improve the quality of the paper. The authors are grateful for funding from the University of KwaZulu-Natal.

Author Contributions

Conceived and designed the experiments: SM NH PS. Analyzed the data: SM NH PS. Wrote the paper: SM.

References

1. Gupta AS, Gupta PS (1977) Heat and mass transfer on a stretching sheet with suction and blowing. *Canadian Journal of Chemical Engineering* 55: 744–746. doi: [10.1002/cjce.5450550619](https://doi.org/10.1002/cjce.5450550619)
2. Carragher P, Crane LJ (1982) Heat transfer on a continuous stretching sheet. *Zeit. Angew. Math. Mech.* 62: 564–565. doi: [10.1002/zamm.19820621009](https://doi.org/10.1002/zamm.19820621009)
3. Khan A, Khan I, Ali F, ulhaq S, Shafie S (2014) Effects of wall shear stress on unsteady MHD conjugate flow in a porous medium with ramped wall temperature. *PLoS ONE* 9(3): e90280. doi: [10.1371/journal.pone.0090280](https://doi.org/10.1371/journal.pone.0090280) PMID: [24621775](https://pubmed.ncbi.nlm.nih.gov/24621775/)
4. Samiulhaq, Ahmad S, Vieru D, Khan I, Shafie S (2014) Unsteady magnetohydrodynamic free convection flow of a second grade fluid in a porous medium with ramped wall Temperature. *PLoS ONE* 9(5): e88766. doi: [10.1371/journal.pone.0088766](https://doi.org/10.1371/journal.pone.0088766) PMID: [24785147](https://pubmed.ncbi.nlm.nih.gov/24785147/)
5. Khalid A, Khan I, Shafie S (2015) Exact solutions for free convection flow of nanofluids with ramped wall temperature. *Eur. Phys. J. Plus* 130: 57 doi: [10.1140/epjp/i2015-15057-9](https://doi.org/10.1140/epjp/i2015-15057-9)
6. Wang CY (1984) The three dimensional flow due to a stretching flat surface. *Phys. Fluids* 27: 1915–1917. doi: [10.1063/1.864868](https://doi.org/10.1063/1.864868)
7. Hussanan A, Ismail Z, Khan I, Hussein AG, Shafie S (2014) Unsteady boundary layer MHD free convection flow in a porous medium with constant mass diffusion and Newtonian heating. *Eur. Phys. J. Plus* 129: 46. doi: [10.1140/epjp/i2014-14046-x](https://doi.org/10.1140/epjp/i2014-14046-x)
8. Pavlov KB (1974) Magnetohydrodynamic flow of an incompressible viscous fluid caused by the deformation of a plane surface. *Magnitnaya Gidrodinamika* 4: 146–147.
9. Mabood F, Khan WA, Ismail AIM (2013) Optimal homotopy asymptotic method for flow and heat transfer of a viscoelastic fluid in an axisymmetric channel with a porous wall. *PLoS ONE* 8(12): e83581. doi: [10.1371/journal.pone.0083581](https://doi.org/10.1371/journal.pone.0083581) PMID: [24376722](https://pubmed.ncbi.nlm.nih.gov/24376722/)
10. Homann F (1936) Der Einfluss grosser Zahigkeit bei der stromung um den Zylinder und um die Kugel. *Zeit. Angew. Math. Phys.* 16: 153–164. doi: [10.1002/zamm.19360160304](https://doi.org/10.1002/zamm.19360160304)
11. Chiam TC (1994) Stagnation-point flow towards a stretching plate. *J. Phys. Soc. Japan* 63: 2443–2444. doi: [10.1143/JPSJ.63.2443](https://doi.org/10.1143/JPSJ.63.2443)
12. Mahapatra TR, Gupta AS (2003) Stagnation-point flow towards a stretching surface, *Can. J. Chem. Eng.* 81: 258–263.
13. Attia HA (2007) Axisymmetric stagnation point flow towards a stretching surface in the presence of a uniform magnetic field with heat generation. *Tam. J. Sci. Eng.* 10(1): 11–16.
14. Miklavcic M, Wang CY (2006) Viscous flow due to a shrinking sheet. *Quart. Appl. Math.* 64(2): 283–290. doi: [10.1090/S0033-569X-06-01002-5](https://doi.org/10.1090/S0033-569X-06-01002-5)
15. Wang CY (2008) Stagnation flow towards a shrinking sheet. *Int. J. Nonlinear Mech.* 43: 377–382. doi: [10.1016/j.ijnonlinmec.2007.12.021](https://doi.org/10.1016/j.ijnonlinmec.2007.12.021)

16. Qasim M, Khan I, Shafie S (2013) Heat transfer in a micropolar fluid over a stretching sheet with Newtonian heating. *PLoS ONE* 8(4): e59393. doi: [10.1371/journal.pone.0059393](https://doi.org/10.1371/journal.pone.0059393) PMID: [23565151](https://pubmed.ncbi.nlm.nih.gov/23565151/)
17. Mahapatra TR, Nandy SK (2013) Momentum and heat transfer in MHD axisymmetric stagnation-point flow over a shrinking sheet. *Journal of Applied Fluid Mechanics* 6 (1): 121–129.
18. Qayyum M, Khan H, Rahim MT, Ullah I (2015) Modeling and analysis of unsteady axisymmetric squeezing fluid flow through porous medium channel with slip boundary. *PLoS ONE* 10(3): e0117368. doi: [10.1371/journal.pone.0117368](https://doi.org/10.1371/journal.pone.0117368) PMID: [25738864](https://pubmed.ncbi.nlm.nih.gov/25738864/)
19. Mabood F, Khan WA, Ismail AIM (2015) MHD boundary layer flow and heat transfer of nano fluids over a nonlinear stretching sheet: A numerical study. *Journal of Magnetism and Magnetic Materials* 374: 569–576. doi: [10.1016/j.jmmm.2014.09.013](https://doi.org/10.1016/j.jmmm.2014.09.013)
20. Mabood F, Khan WA, Uddin MJ, Ismail AIM (2015) Optimal homotopy asymptotic method for MHD slips flow over a radiating stretching sheet. *Far East Journal of Applied Mathematics* 90(1): 21–40. doi: [10.17654/FJAMJan2015_021_040](https://doi.org/10.17654/FJAMJan2015_021_040)
21. Mabood F, Khan WA, Ismail AIM (2015) MHD stagnation point flow and heat transfer impinging on stretching sheet with chemical reaction and transpiration. *Chemical Engineering Journal* 273: 430–437. doi: [10.1016/j.cej.2015.03.037](https://doi.org/10.1016/j.cej.2015.03.037)
22. Khan JA, Mustafa M, Hayat T, Alsaedi A (2014) On three-dimensional flow and heat transfer over a non-linearly stretching sheet: analytical and numerical solutions. *PLoS ONE* 9(9): e107287. doi: [10.1371/journal.pone.0107287](https://doi.org/10.1371/journal.pone.0107287) PMID: [25198696](https://pubmed.ncbi.nlm.nih.gov/25198696/)
23. Bansal JL (1994) Magnetofluidynamics of viscous fluid. Jaipur Publishing House, Jaipur, India.
24. Jat RN, Rajotia D (2014) Effects of partial slip on three dimensional MHD viscous flow and heat transfer due to a permeable Axisymmetric shrinking sheet with viscous dissipation and heat source/sink. *Thermal Energy and Power Engg.* 3(2) 234–244.
25. Chiam TC (1998) Heat transfer in a fluid with variable thermal conductivity over stretching sheet. *Acta Mechanica* 129: 63–72. doi: [10.1007/BF01379650](https://doi.org/10.1007/BF01379650)
26. Shercliff JA (1965) A Textbook of Magnetohydrodynamics. Oxford, Pergamon Press.
27. Motsa SS (2013) A New spectral relaxation method for similarity variable nonlinear boundary layer flow systems. *Chemical Engineering Communications* 16: 23–57.
28. Motsa SS, Dlamini PG, Khumalo M (2014) Spectral relaxation method and spectral quasilinearization method for Solving Unsteady Boundary Layer Flow Problems. *Advances in Mathematical Physics*, Article ID 341964, 12: doi: [10.1155/2014/341964](https://doi.org/10.1155/2014/341964)
29. Motsa SS, Makukula ZG (2013) On spectral relaxation method approach for steady von Karman flow of a Reiner-Rivlin fluid with Joule heating and viscous dissipation. *Central European Journal of Physics* 11: 363–374.
30. Fang T, Zhang J, Yao S (2009) Viscous flow over an unsteady shrinking sheet with mass transfer. *Chinese Physics Letters* 26 (1): 014703. doi: [10.1088/0256-307X/26/1/014703](https://doi.org/10.1088/0256-307X/26/1/014703)
31. Rohni AM, Ahmad S, Ismail AI, Pop I (2013) Flow and heat transfer over an unsteady shrinking sheet with suction in a nanofluid using Buongiorno's model. *International Communications in Heat and Mass Transfer* 43: 75–80. doi: [10.1016/j.icheatmasstransfer.2013.02.001](https://doi.org/10.1016/j.icheatmasstransfer.2013.02.001)
32. Nandy SK, Sumanta S, Mahapatra TR (2014) Unsteady MHD boundary-layer flow and heat transfer of nanofluid over a permeable shrinking sheet in the presence of thermal radiation. *Alexandria Engineering Journal* 53: 929–937. doi: [10.1016/j.aej.2014.09.001](https://doi.org/10.1016/j.aej.2014.09.001)
33. Rahimpour M, Mohebpour SR, Kimiaeifar A, Bagheri GH (2008) On the analytic solution of axisymmetric stagnation flow towards a shrinking sheet. *International Journal of Mechanics* 1(2): 1–10.